Topics in Catalysis (2020) 63:451–467
https://doi.org/10.1007/s11244-020-01242-x

ORIGINAL PAPER

Synthesis of 10 and 12 Ring Zeolites (MCM-22, TNU-9 and MCM-68) Modified with Zn and Its Potential Application in the Reaction of Methanol to Light Aromatics and Olefins

Misael García-Ruiz[1] · Dora A. Solís-Casados[2] · Julia Aguilar-Pliego[3] · Carlos Márquez-Álvarez[4] · Enrique Sastre-de Andrés[4] · Diana Sanjurjo-Tartalo[4] · Raquel Sáinz-Vaque[4] · Marisol Grande-Casas[4]

Published online: 17 February 2020

Abstract

The effect on the incorporation of zinc of three zeolites TNU-9, MCM-22, and MCM-68 was investigated. The physicochemical properties of zeolites were studied by X-ray diffraction, N_2-adsorption, temperature-programmed desorption of NH_3 (TPD), nuclear magnetic resonance of ^{27}Al and ^{29}Si (MAS NMR), scanning electron microscopy (SEM) and thermogravimetric analysis (TGA). Then all the samples were characterized and evaluated in the reaction of methanol to aromatics (MTA). The correlation of zinc incorporation method and acidic properties of zeolites with catalytic performance was investigated. The form of zinc incorporation, the acidity, the type of zeolitic structure and the reaction temperature had a great influence on the catalytic activity. Regarding the type of structure, the total aromatics selectivity in this work increased in the followed order for zeolites modified with Zn: MCM-68 > TNU-15 > MCM-22. The medium pore zeolite T9-15 (TNU-9 zeolite and Si/Al 15 ratio) catalysts with the ratio $ZnO/ZnO + Al_2O_3$ equal to 0.34 (T9-15 0.5 Zn) showed better stability with conversion of methanol completes during 9 h of reaction and 17% to BTX selectivity and 32% to total aromatics compounds at 450 °C and WHSV of 4.24 h^{-1}. In methanol conversion, the selectivity to aromatics over the T9-15 modified-Zn materials (TNU-9 zeolite and Si/Al 15 ratio) under study, increased in the followed order: T9-15 0.5 Zn > ZT9-15 > T9-15 > T9-15 0.2 Zn. The reaction temperature is an important variable in the MTA process. At 450 °C a better activation of acid sites is achieved in zeolite with Zn and therefore a high percentage of BTX selectivity is obtained for TNU-9 zeolite.

Keywords Methanol conversion · Aromatics compounds · BTX fraction · Zeolites modified · Light olefins

1 Introduction

Zeolites are crystalline aluminosilicate constituted by silica tetrahedron and alumina tetrahedron through oxygen bridges containing ordered micropores that enable shape-selective transformation [1]. Because of its high thermal stability and strong Brønsted acidity of zeolite catalysts, gives rise to many applications, for example in isomerization [2], alkylation [3] and aromatization reactions [4].

The conversion of methanol to hydrocarbons (MTH) over acidic zeolites has drawn considerable attention since its discovery in 1970s by Mobil Corporation. Depending on the product of reaction selectivity, this process was named as MTG (methanol to gasoline), MTO (methanol to olefins), MTP (methanol to propene) and MTA [methanol to aromatics (MTA)]. In this last process, aromatic compounds, especially benzene, toluene and xylene (BTX fraction) and light olefins, such as ethene and propene, are mainly produced

Electronic supplementary material The online version of this article (https://doi.org/10.1007/s11244-020-01242-x) contains supplementary material, which is available to authorized users.

✉ Misael García-Ruiz
misagr89@gmail.com

[1] Doctorado en Ciencia de Materiales de La Facultad de Química, Universidad Autónoma del Estado de México, Paseo Colón Esquina Paseo Tollocan S/N, C.P. 50000 Toluca, Estado de México, Mexico

[2] Universidad Autónoma del Estado de México, Centro Conjunto de Investigación en Química Sustentable UAEM-UNAM, Personal Académico Adscrito a La Facultad de Química, UAEMex, Toluca, Estado de México, Mexico

[3] Área de Química Aplicada, Departamento de Ciencias Básicas, UAM-A, San pablo 180, C.P. 02200 Cuidad de México, Mexico

[4] Instituto de Catálisis y Petroleoquímica, CSIC, C/Marie Curie 2, Campus Cantoblanco, 28049 Madrid, Spain

from the oil-based route to this date, the gradual depletion of oil reserves has resulted in a sustained tight supply and high cost of aromatics [5]. In recent years, the conversion of MTA has attracted great attentions because methanol can be easily produced via syngas from various sources, such as biomass, natural gas and coal [6]. One process that uses zeolites as shape-selective catalysts is the conversion of MTA and light olefins (MTO). For these methanol conversion technologies, ZSM-5 zeolite has been considered as an important catalyst [7]. As a crystalline aluminosilicate, ZSM-5 zeolite has well-defined microporous structure, large surface area and strong acidity [8], which contributes to high activity and selectivity for hydrocarbon production in MTH reaction [9]. In a previous article [10] we demonstrate the high catalytic activity of the modified-Zn ZSM-5 zeolite in the MTA process. The Zn/ZSM-5 catalyst obtained complete methanol conversions and high selectivity to the BTX fraction. On the other hand, we show that the crystal size has a significant influence on the catalytic activity improving the useful life of the catalyst. The ZSM-5 nanocrystalline zeolite showed a BTX selectivity of 32% with 80% conversions until 9 h reaction.

As demonstrated in previous studies [11], certain medium pore zeolites (with 10 and 12-membered channels), doped with different metals include Zn, La, Ga, Ag, Cu, Sn, Ni, Mo and Cr are capable of transforming methanol, however, the selectivity to a specific product versus time is different in each case. Furthermore, it has been widely accepted that Zn species could greatly increase the selectivity of BTX in MTA reaction compared with other metal species. Specifically, Zn can be incorporated into zeolite by two methods; ion exchange (i) or in the synthesis gel (G) [12].

In this study, comprising different combinations of 10- and 12-ring pores, namely MCM-22 (MWW), TUN-9 (TNU) and MCM-68 (MSE), which have not been little studied in this type of reactions. Catalyst MCM-22 (MWW topology), which has unique pore architecture with two independent pore systems, 0.41 nm × 0.51 nm 2D (two-dimension) 10-ring sinusoidal pore system and large 3D 12-ring supercage system connected by 0.40 nm × 0.55 nm 10-ring windows The unique structure and the presence of supercage in MWW-type zeolites are considered essential in promoting activity and stability of the catalyst in methanol conversion reactions [13]. MCM-68 (framework type code: MSE) is a multipore zeolite with three-dimensional 2 × 10 × 10-ring channel system, including a 12-ring (6.4 × 6.8 Å) straight channel and two tortuous 10-ring (5.2 × 5.8 Å and 5.2 × 5.2 Å) channels that intersect with each other [14]. Its four 10-ring windows may make H-MCM-68 more resistant to coke formation, because of their connection into the large 12-ring channels [15]. Finally, TNU-9 (Taejon National University No. 9), a new high-silica zeolite with 3D 10-ring channel system, has previously been synthesized by Suk Bong Hong et al. [16]. TNU-9 (TUN topology) consists of two different types of straight 10-ring channels running parallel to y-axis, with the dimension of 5.5 × 6.0 and 5.2 × 6.0 Å. The channels perpendicular to y-axis join these straight channels to form a 3D 10-ring channel system [17].

Due to the peculiar pore structure of these zeolites have been applied in many catalytic processes and is a potential catalyst in MTA and MTO reaction. Specifically, Zhang et al. [18] investigated H-MCM-22 catalyst in MTO reaction, they showed the light olefin selectivity seems to be related to the amounts of Brønsted acid, a comparison of Lewis acid which does not benefit to improve the catalytic stability. However, an important difficulty that a zeolite catalyst encounters is the heavy coke formation in the reaction process obtaining both longer lifetime and higher BTX selectivity is difficult. Therefore, the main challenge of our work is to improve the lifetime of the catalyst and produce high selectivity to aromatics. In this work, the effects of Zn incorporation and reactions on the catalytic performance of a Zn-modified of the three types of zeolites with different ration Si/Al in methanol conversion were investigated.

2 Experimental

2.1 Materials

The reagents used for the preparation of zeolites are tetraethyl orthosilicate (TEOS, 98%, Aldrich), fumed silica (Aerosil 200, Degussa), sodium hydroxide (NaOH), sodium aluminate (41 wt%Al_2O_3, 37 wt% Na_2O), Bicyclo[2.2.2]oct-7-ene-2,3,5,6-tetracarboxylic dianhydride (> 95.0%, Sigma-Aldrich), hexamethyleneimine (HMI, 99%, Sigma Aldrich), aluminum hydroxide hydrated ($Al(OH)_3$, Sigma-Aldrich), colloidal silica (40 wt% suspension in H_2O, LUDOX HS-40, Aldrich), Zinc nitrate hexahydrate ($Zn(NO_3)_2 1{\cdot}6H_2O$ reagent grade, 98%, Sigma-Aldrich), Aluminium nitrate ($Al(NO_3)_3{\cdot}9H_2O$ ACS reagent, ≥ 98%, Sigma-Aldrich), 1,4-dibromobutane (99%, Aldrich), 1-methylpyrrolidine (97%, Aldrich), methanol HPLC, ≥ 99.9% (Sigma-Aldrich) and Zinc acetate dihydrate ($Zn(CH_3COO)_2{\cdot}2H_2O$, 99% Sigma Aldrich).

2.2 Synthesis of MCM-22 Zeolite

A sample of zeolite MCM-22 with Si/Al ratio of 30 and 50 was synthesized following the procedure described by Wu et al. [19] with some modifications. The gel was prepared with the molar composition $xSiO_2$: yAl_2O_3:0.075 Na_2O: 0.6 HMI: zZnO:35 H_2O, where x/y is ration Si/Al (30 and 50) and z represents the moles of Zn (in your case). First, sodium hydroxide and sodium aluminate were dissolved in deionized water in a Teflon glass and $Zn(NO_3)_2{\cdot}6H_2O$ (in the case).

Once dissolved, hexamethyleneimine (HMI) was added as structure directing agent (SDA) and finally was added fumed silica. The resulting mixture was vigorously shaken for 2 h to room temperature, after what the mixture was distributed in Teflon-lined, stainless steel autoclaves and heated at 160 °C for 11 days, both in conditions of agitation at 60 rpm (A) and in static conditions (S). After this period the autoclaves were removed from the oven, quenched in ice and the solid was filtered and washed with deionised water until pH 7. The product was dried at 110 °C overnight and calcined at 550 °C for 20 h in air atmosphere.

2.3 Synthesis of MCM-68 Zeolite

MCM-68 zeolite was synthesized according to previous literature [20]. The SDA, *N*,*N*,N_0,N_0-tetraethylbicyclo[2.2.2] oct-7-ene-2,3:5,6- dipyrrolidinium diiodide ($TEBOP^{2+}(I^-)_2$) was synthesized exactly following the reported procedure [21] from commercially available bicyclo[2.2.2]oct-7-ene-2,3:5,6-tetracarboxylic anhydride (Aldrich) by three steps in 58% overall yield. The typical gel composition is $xSiO_2$:0.1$TEBOP^{2+}(I^-)_2$:0.375KOH:y$Al(OH)_3$:30H_2O, where x/y represents the Si/Al molar ratio of 11. In a typical synthesis, colloidal silica, distilled water, and $Al(OH)_3$ were mixed and stirred at room temperature for 10 min, then KOH was added to the solution and stirred for another 15 min. After that, $TEBOP^{2+}(I^-)_2$ was added and the mixture was stirred for 3 h. Then the gel was transferred to a 50 mL Teflon-lined autoclave and placed in a 160 °C oven for 14 days in static conditions. The solid product obtained was separated by filtration, washed several times with distilled water, and dried overnight. The as-synthesized MCM-68 was calcined in a muffle furnace at 650 °C for 6 h to remove the SDA.

2.4 Synthesis of TNU-9 Zeolite

TNU-9 zeolite was synthesized under hydrothermal conditions following the procedure given by Hong et al. [17] using 4-bis(methylpyridinium) pentane (1,4-MPP) as organic structure-directing agent (SDA). (1,4-MPP) in its bromide forms was prepared, purified, and characterized as described in previous paper [22]. This diquaternary ammonium salt was stored in a desiccator for use as an SDA.

In a typical synthesis, $Al(NO_3)_3{\cdot}9H_2O$ (98%, Sigma Aldrich) and NaOH (98%, Sigma Aldrich) were dissolved in deionized water in a Teflon glass, and the mixture was vigorously stirred for 2 h, (1,4-MPP) was added once dissolved, fumed silica was added as a source of silica, the gel was mixed vigorously for 2 h at room temperature. The gel was placed in autoclaved at 160 °C with continuous stirring at 60 rpm for 10 days. The final synthesis gels had the following chemical composition: $xSiO_2$: 11Na_2O: yAl_2O_3: 4.5(1,4-MPP): 1200H_2O, where x/y represents the Si/Al molar ratio of 15, 30 and 50. The solid was recovered by filtration, dried at 70 °C and was calcined under flowing air at 550 °C for 10 h to remove the occluded organic SDA.

On the other hand, the synthesis of zinc-substituted TNU-9 zeolites was performed using the previous procedure, however, the final composition of the gel was 30 SiO_2: 11 Na_2O: xZnO: yAl_2O_3: 4.5 (1,4-MPP): 1200H_2O, where x is the amount of zinc oxide placed in the synthesis gel using zinc acetate dihydrate ($Zn(CH_3COO)_2{\cdot}2H_2O$, 99% Sigma Aldrich) and Si/Al 15 ration. For these gels, the amount of ZnO was varied for a x/x + y of 0.33 y 0.16 ration, which corresponds to 0.5 and 0.2 mol of ZnO, respectively.

2.5 Preparation of Acid Zeolites H-MCM-22, H-MCM-68 and H-TNU-9 and Ion Exchange with Zn

The Na-Zeolites were converted to H-Zeolites (acid form) by refluxing twice with 1 M NH_4NO_3 solution at 80 °C for 3 h, followed by filtered and drying at 110 °C over night and calcination at 550 °C for 4 h in air. The acid zeolites previously synthesized were exchanged with a 0.025 M solution of $Zn(NO_3)_2{\cdot}$6H2O at 80 °C for 4 h. The zeolite was filtered, washed and dried at 70 °C, finally the resulting powder was calcined at 550 °C for 4 h with air flow. Table 1 lists the results from syntheses performed and its conditions.

2.6 Catalyst Characterization

Powder X-ray diffraction (PXRD) patterns were collected with an XPert Pro PANalytical diffractometer (CuKα1 radiation = 0.15406 nm). Scanning electron microscopy (SEM) images were recorded on a Hitachi S-3000 N microscope. Transmission electron microscopy (TEM) study was carried on a JEOL 2100F microscope opening to 200KV. Nitrogen adsorption/desorption isotherms were measured at − 196 °C in a Micromeritics ASAP 2020 device. Before the measurement, the previously calcined sample was degassed at 350 °C under high vacuum for at least 10 h. Surface areas were estimated by the BET method whereas microporous and external surface areas were estimated by applying the t-plot method.

Solid-state magic-angle spinning (MAS) NMR experiments were conducted on a Bruker Avance 300 (11.75 T) spectrometer operated with frequency at 130.32 MHz and spinning rate at 10 kHz. The 27Al NMR spectra were recorded using a pulse width of 0.5 µs (π/12 flip angle), 2400 scans and a recycle delay of 1 s.

The Al, Si and Zn concentrations of samples were obtained by inductively coupled plasma-optical emission spectroscopy (ICP-OES) with a Optima 3300 DV Perkin Elmer. Temperature programmed desorption of ammonia

Table 1 Synthesized zeolites and their synthesis conditions

Zeolite	Ration Si/Al	Synthesis conditions	Zn incorporation method	Denoted
MCM-22	30	Agitation	Synthesis gel	M22-30A-G
	30	Static	Synthesis gel	M22-30S-G
	30	Static	Ion exchange	ZM22-30S
	30	Static	Synthesis gel	ZM22-30S-G
	30	Agitation	Ion exchange	ZM22-30A
	50	Agitation	N/A	M22-50A
	50	Static	N/A	M22-50S
MCM-68	11	Static	Ion exchange	ZM68-11
TNU-9	15	Agitation	N/A	T9-15
	15	Agitation	Ion exchange	ZT9-15
	15	Agitation	Synthesis gel	T9 0.5 Zn
	15	Agitation	Synthesis gel	T9 0.2 Zn
	30	Agitation	N/A	T9-30
	30	Agitation	Ion exchange	ZT9-30
	50	Agitation	N/A	T9-50
	50	Agitation	Ion exchange	ZT9-50

(NH_3-TPD) was conducted using a Micrometrics Autochem II chemisorption analysis equipment. Typically, 100 mg of sample pellets (30–40 mesh) were pretreated at 550 °C for 1 h in helium flow (25 mL/min) and then cooled to the adsorption temperature (177 °C). A gas mixture of 5.0 vol% NH_3 in He was then allowed to flow over the sample for 4 h at a rate of 15 mL/min. Afterwards, the sample was flushed with a 25 mL/min helium flow for 30 min while maintaining the temperature at 177 °C to remove weakly adsorbed NH_3, and finally the temperature was increased to 550 °C at a rate of 10 °C/min. Thermogravimetric analysis (TGA) were carried out at a heating of 30 °C to 900 °C with a rate of 20 °C/min under air flow and registered in a PerkinElmer TGA7 instrument.

2.7 MTA Catalytic Testing Conditions

Zn modified zeolites were tested as catalysts in the conversion of methanol at different reaction temperatures at 400, 425 and 450 °C in a Microactivity reaction set (PID Eng & Tech) consisting of a fixed bed reactor completely automated and controlled from a computer. The reactor outlet is connected to a gas chromatograph to analyze the reaction products. N_2 was used as a stripping gas under a controlled flow. The methanol was fed as a liquid using an HPLC pump (Gilson 307). The methanol was converted to the gas phase and mixed with the N_2 stream in a preheater at 180 °C to generate a gas mixture with a constant molar ratio of methanol/N_2 of 4. Before the reaction, the catalysts were activated at 550 °C for 1 h low air flow to remove any trace of organic molecules or moisture adsorbed within the pores of the catalyst. Typically, the sample was compacted and sieved in a 20–30 mesh, corresponding to a particle size between 0.84 and 0.59 mm. The weight of the catalyst and the flow of methanol were optimized to achieve different values of space velocities (WHSV).

The reaction products were analyzed online by gas chromatography with a VARIAN CP3800 chromatograph. The device is equipped with two columns: (i) a Petrocol DH50.2 capillary column connected to an FID detector, and (ii) a Porapack Q 80–100 mesh packed column (2 m length, 3.17 mm (1/8") diameter external and 2 mm internal diameter) connected to a TCD detector, to analyze hydrocarbons and oxygenated products, respectively.

3 Results and Discussion

3.1 X-Ray Diffraction

Figure 1a shows that all the parent H-MCM-22 and modified-Zn samples have a typical MWW structure [18]. H-MCM-22 zeolites with different methods of Zn incorporation display high intensities of the XRD patterns, showing high crystallinity, a diffraction line at $2\theta = 7.08°$ associated to 0 0 2 diffraction plane, characteristic of a layered structure of MWW sheets stacking along the c-direction, is observed. Three well resolved diffraction lines due to 1 0 0, 1 0 1 and 1 0 2 planes are also detected. Concerning the M22-30S product, the presence in its XRD pattern of an intense peak at $2\theta = 9.45$, 22.4 and 25.7°, suggests that, besides MCM-22, another phase is formed during crystallisation. It is known [23, 24], formation of ferrierite phase besides MCM-22 has been reported over static synthesis conditions. Figure 1b presents XRD patterns for TUN zeolites synthesized with different Si/Al ratios (15, 30 and 50)

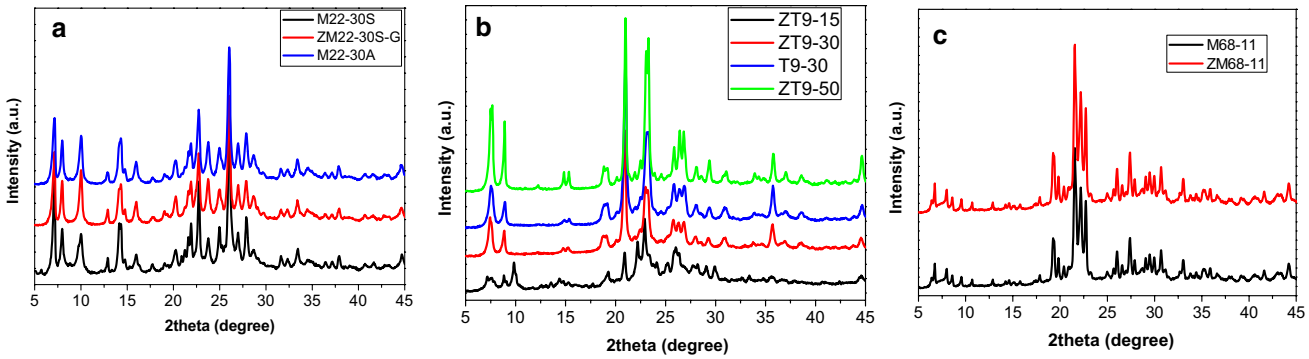

Fig. 1 XRD patterns of HMCM-22, HMCM-68 and HTNU-9 zeolites selected

exchanged with Zn and the acid sample T9-30 to verify there is not characteristic peaks of ZnO suggesting that Zn species were highly dispersed on TNU-9 zeolite [25]. All four X-ray patterns evidence high crystallinity and phase purity of these samples confirming that no structural changes proceeded during the post-synthesis treatments. The structure of zeolites was preserved after all treatments with Zn and no significant changes were observed in the individual XRD patterns. The XRD patterns of different MCM-68 samples are presented in Fig. 1c. The zeolites of as-synthesized M68-11 and ZM68-11 showed a typical MSE topology with good crystallinity. The XRD patterns of ZM68-11 sample was consisted of the typical reflections at 6.79°, 8.06°, 9.66°, 19.36°, 21.62°, 22.50°,26.14° and 27.50°. MSE topology with Zn no obvious decrease in crystallinity compared with M68-11, suggesting that ZM68-11 zeolite structure was very well preserved after treatment [26].

3.2 N_2 Adsorption–Desorption

The N_2 adsorption–desorption isotherms of all MCM-22 modified samples are shown in Fig. 2a. All the curves can be classified as a type I + IV isotherm, pointing out that in these solids, along with the characteristic microporous zeolite framework there is a mesoporous structure. Nitrogen adsorption–desorption isotherms of TNU-9 acids and modified with Zn are shown in Fig. 2b. The TNU-9 samples show the type I isotherm with a high nitrogen uptake at low relative pressures, which is characteristic for purely microporous materials [27].

The adsorption isotherms did not practically change their shape and all samples possess practically the same micropore volume (0.107–0.152 cm^3/g). The distinctive increase in adsorption capacity at p/po = 0.4–0.9, reveals that the presence of mesopores, whereas ZT9-15 sample shows an increase in quantity adsorbed at high pressures due to the presence of crystals of smaller size as observed by SEM. Finally, N_2 adsorption–desorption isotherms of various zeolites are shown in Fig. 2c. Clearly, ZM68-11 exhibited type I isotherm with a very steep rise in N_2 amount adsorbed in the low relative pressure (p/po) range and a small hysteresis loop of type H3 in the high p/po range of 0.9–1.0, indicating its typical microporous feature as well as the existence of some mesopores and/or macropores derived mainly from the pile-up of zeolite crystals [20].

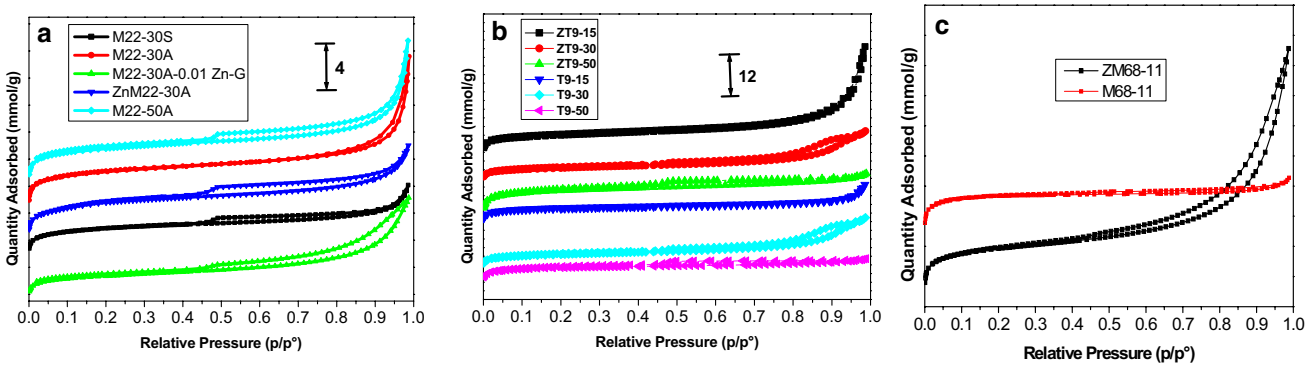

Fig. 2 N_2 adsorption–desorption isotherms **a** MCM-22, **b** TNU-9 and **c** MCM-68 zeolites

BET surface areas, microporous surface areas, microporous volumes and external surface areas of acid zeolites and exchanged zeolites are listed in Table 2. Both the surface area and total pore volume decreased after zinc treatment, suggesting that species ZnO may have been highly dispersed on the external surfaces or in the channels of the zeolites, especially for ZM22-30A-G (232 $m^2\ g^{-1}$) by direct synthesis and ZT9-50 (312 $m^2\ g^{-1}$) by ion exchange. TUN-9 samples the surface area and the micropore volume decrease as the Si/Al ratio increases. The large surface area is the result of a purely microporous framework with molecular dimensions for shape selectivity which is a characteristic of zeolites. A large external surface area produces to number of pore mouths and increase the accessibility of acid sites in the micropores, which delay the deactivation by coke formation [28].

Table 2 Textural properties of zeolites prepared

Catalyst	$S_{BET}/m^2/g$	S micro/ m^2/g	$S_{external}/m^2/g$	Vmicro/cm^3/g
M22-30A	526	453	73	0.191
M22-30S	356	301	55	0.132
ZM22-30AG	232	48	184	0.0717
ZM22-30S	208	161	47	0.0633
M22-50A	450	64	386	0.1484
M22-50S	324	121	203	0.0809
ZM22-50S	469	381	88	0.1477
M68-11	610	578	32	0.2173
ZM68-11	429	348	81	0.1349
T9-15	484	414	70	0.1596
ZT9-15	517	401	116	0.1597
T9 0.5 Zn	320	250	70	0.0978
T9 0.2 Zn	470	395	75	0.1524
T9-30	361	268	92	0.1058
ZT9-30	361	276	85	‘0.1083
T9-50	346	308	38	0.1176
ZT9-50	312	269	43	0.1035

The surface area and micropore volume of these zeolites are listed in Table 2, which were calculated using the BET and t-plot methods, respectively. The large surface area is the result of a purely microporous framework with molecular dimensions for shape selectivity. The external surface area and micropore surface area of zeolites all decreased after the introduction of Zn species, indicating the Zn species were loaded on the external surface and into the channels of Zn modified zeolites simultaneously [24, 26].

3.3 Scanning Electron Microscopy (SEM)

SEM images of MCM-22 samples in stirring conditions are shown in Fig. 3. For the M22-30A samples the SEM images confirm the crystallisation of pure MCM-22 in such conditions, which appears in the form of very thin particles in the form of a rose forming relatively small lamellar particles [24]. However, the samples synthesized hydrothermally in static conditions show different morphology (Fig. 4). The samples have a morphology spherical particle with a small hole at the center due to the coupling of sheets of structure MWW. Previous reports show that the conditions of synthesis drastically influence the morphology of the MCM-22 zeolites. Scanning electron images of parent and modified TUN zeolites are given in Fig. 5. The SEM pictures of ZT9-15 show a rod-like morphology and a crystal size in the range of 1–1.5 µm (Fig. 5a). The ZT9-30 sample present 0.2 m spherical crystallites formed by stacked sheets (Fig. 5b). Finally, sample ZT9-50 shows a totally different morphology, large crystals of 16 µm with intercrystalline

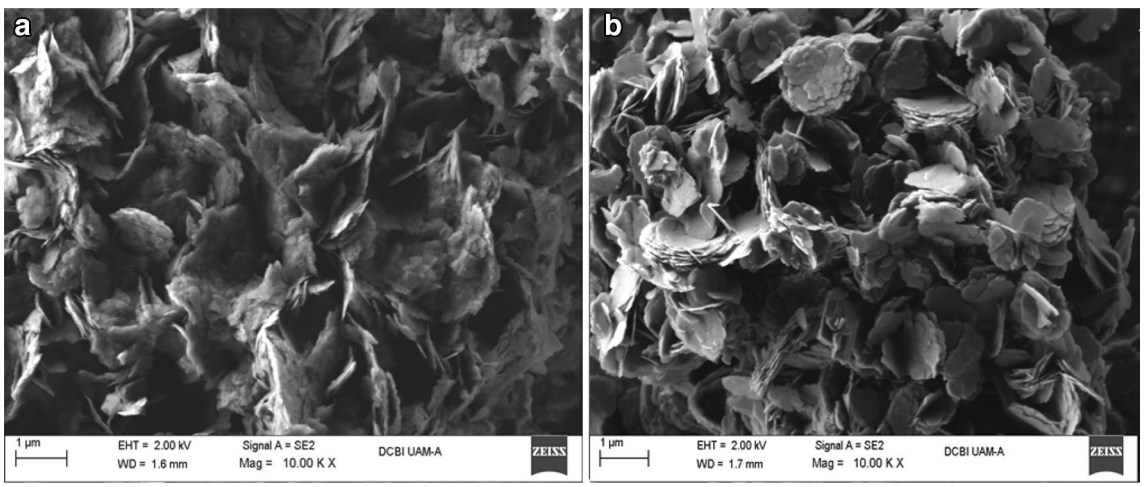

Fig. 3 SEM images of the M22-30A samples (stirring conditions)

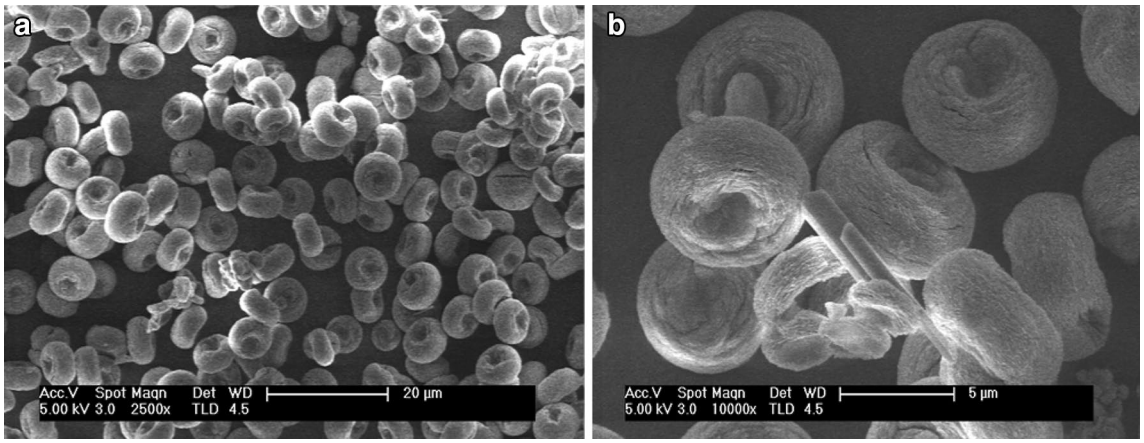

Fig. 4 SEM images of the M22-30S sample (static conditions)

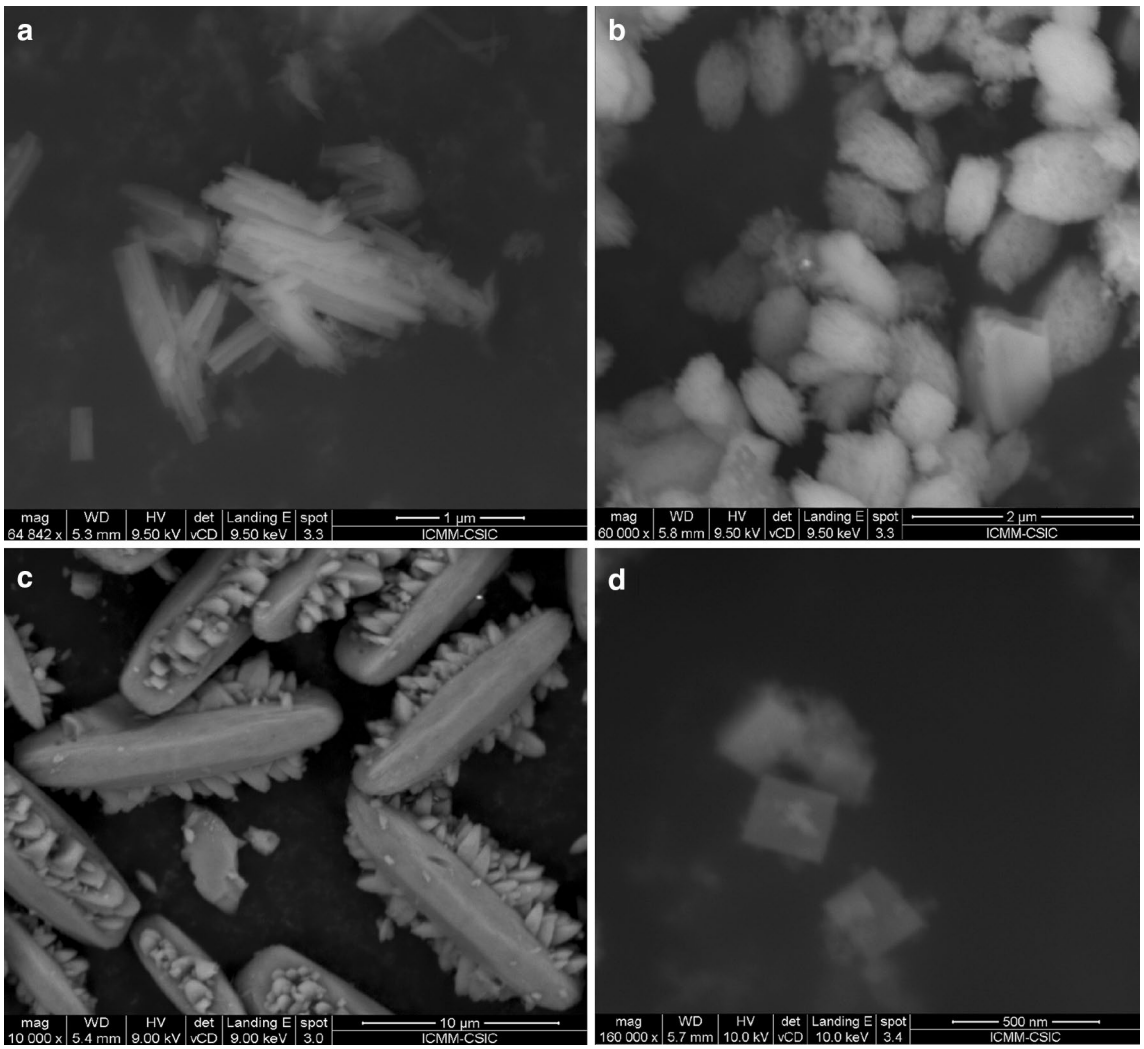

Fig. 5 SEM images of the samples: **a** ZT9-15, **b** ZT9-30, **c** ZT9-50 and **d** ZM68-11

growths inside them. The large crystals of this catalyst tend to have an inefficient diffusion of reactant molecules and products in the MTA process. The ration Si/Al influences in a considerate way distribution of crystals sizes and shapes of TUN zeolite (Fig. 5c). Figure 5d shows the SEM images of these MSE type zeolites. It could be found that ZM68-11 exhibited cuboid shaped crystallites with sizes of about 100–200 nm, which was like the previous report [26]. In this study, the crystal size decreased in the order ZM68-11 > ZT9-15 > M22-30A which is also in agreement with the observed relative stability.

3.4 Thermogravimetric Analyses (TGA) and Derivate (DTA)

The ATG/DTG curves of all zeolites not calcined are shown in Fig. 6a and b, respectively. Firstly, the ATG of the zeolite M22-30A without calcined (black line) presents a small mass loss to lower than 100 °C, correspond to adsorption water retained in the samples. The weight loss that appears between 250 and 550 °C was due to oxidative decomposition of structure directing agent (hexamethyleneimine), which occurs in three steps. The first stage at 245 °C corresponds to the decomposition of imine occluded in the pores of zeolite MCM-22 with a percentage of weight loss of 3.75%. The second weight loss (2.18%) at 325 °C is due to the decomposition of the imine that acts as a load compensator in the zeolitic structure. The last loss occurs due to the oxidation of different condensation products within the structure of the MCM-22 with a weight loss greater than 11.61%.

In the air TGA of the M68-11 zeolite (blue line) prior to calcination (Fig. 6b), three maxima were observed at 340, 450 and 645 °C, which agrees with previous reports [29]. These weight losses are due to exothermic processes produced by the combustion of SDA in the air atmosphere. A similar case occurred with the sample not calcined T9-15 (red line), where it had three weight losses at 175, 320 and 492 °C as a result of SDA combustion. The ATG y DTG results of the zeolites after the calcination process are presented in Figure S1a and S1b (Supplementary Information S1), respectively. In all cases a single loss of mass less than 100 °C is observed, which corresponds to the physisorption of water retained in the samples. No other significant weight losses are observed at higher temperature which indicates that the SDA was eliminated.

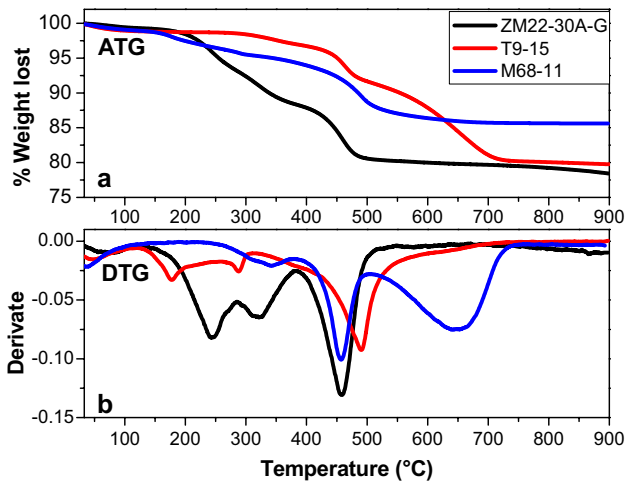

Fig. 6 Thermal analysis of three structure zeolitic not calcined: **a** ATG and **b** DTG

3.5 ICP-OES Chemical Composition Analysis

The amount of Si, Al and Zn in the exchanged zeolites of the calcined samples were determined by ICP-OES analysis (Table 3). It is observed that the incorporation of Zn is efficient both by ion exchange and in the synthesis gel. The concentration of Zn was found to be close to 1% wt in all zeolites modified with Zn both by ion exchange and in synthesis gel. The relation Si/Al to real was measured in all the catalysts, being less than the theoretical in all calcined samples, which suggests that the exchange treatment and subsequent calcination to some extent anneals structural defects and incorporates a part of the extra-framework Al species (Al_{EF}) in the framework again.

Table 3 Chemical composition (wt%) determined by ICP-OES of samples

Catalyst	Theorical ration Si/Al	wt%			Real ration Si/Al
		% Si	% Al	% Zn	
M22-30A	30	36.67	1.20	–	29.65
M22-30S	30	35.92	1.56	–	22.13
ZM22-30S	30	41.08	1.33	0.74	29.78
ZM22-30A-G	30	36.48	1.52	1.20	23.07
M22-50A	50	39.45	0.72	–	52.81
M22-50S	50	39.22	0.90	–	42.06
M68-11	11	34.23	4.02	–	8.12
ZM68-11	11	32.88	4.61	1.11	6.85
T9-15	15	32.92	3.72	–	8.48
ZT9-15	15	33.07	3.92	1.33	8.11
T9 0.5 Zn	15	31.17	3.02	2.11	10
T9 0.2 Zn	15	29.31	4.22	1.53	6.66
T9-30	30	38.07	1.72	–	21.28
ZT9-30	30	36.75	1.22	1.76	28.95
T9-50	50	37.54	0.73	–	49.51
ZT9-50	50	38.54	0.79	0.25	47.01

3.6 Temperature-Programmed Desorption (NH_3-TPD)

The acidic properties of the three zeolite structures modified with Zn were determined by NH_3-TPD technique, as presented in Fig. 7a. The spectra of all samples exhibit two peaks characteristic throughout the temperature range in all zeolites. The low-temperature (LT) region of 200–300 °C and the high temperature (HT) region of 400–500 °C, which are attributed to the NH_3 adsorbed on the acidic hydroxide group Si–OH–Al situated in the framework of zeolite [30]. The TPD profile of ZM22-30A-G (black line) is characterized by one broad and asymmetric desorption peak with maxima in the temperature region 340–350 °C, assignable to NH_3 desorption from strong acid sites [31]. ZT9-15 (red line) shows a peak centered at a temperature of 270 °C and another shoulder with a maximum at approximately 365 °C, the first peak was noted as HL and the second with HT, low and high acidity, respectively. Finally, ZM68-11 zeolite (blue line) presented an intense peak at a temperature of 275 °C, corresponding to weak acidity.

Figure 7b shows NH_3-TPD of TNU-9 modified Zn with different Si/Al ration. We observed that the total acidity increases when the ration Si/Al increases. The peak corresponding to weak acidity (HL) is maintained in the three samples at a temperature between 265 and 275 °C. However, it is clearly observed that increasing the Si/Al ration increases the average acid sites in the sample ZT9-30 until finally a new peak emerges in the sample ZT9-50, which is denoted as peak HT at a temperature of 420 °C. The HT peak above 400 °C is due to the desorption of NH_3 from strong acid sites and these strong adsorption sites of ammonia are active in MTA reactions [32]. The incorporation of zinc species on TNU-9 zeolite exhibits a significant influence on the distribution of strong acid sites. The incorporation of Zn in sample T9-15 decreases the distribution of total acid sites, especially the HT acid sites, as shown in Figure S2a. This indicates that the Zn species should interact poorly with the Brønsted acid sites and generate less amount of acid sites [33].

Figure S2b shows a comparison of the TPD profiles of the zeolite M22-30A and with the zeolite with Zn in the synthesis gel (ZM22-30A-G). It is clearly observed, the intensity of HT peak increased by Zn loading because of the exchange of H^+ with Zn^{2+}, indicating the interaction between the Zn^{2+} ions and Bronsted acid sites on Zn-modified zeolites giving cationic species of Zn, which coordinated with the oxygen atoms in the pore channel [34]. In addition, Xiaoning et al. [35] mentioned that silicon hydroxy and aluminium hydroxy in the zeolite framework were polarized by the polarization and induction of the metal cation. So, the density of the electron cloud in the zeolite framework increased, stronger acidity of the acidic center appeared. These Zn sites can performance as strong sites to catalyze the reaction and obtain high aromatic selectivity. Traditionally, the HT peak is attributed to NH_3 desorption from strong Brønsted and Lewis acid sites, which are associated with the Al_F (framework Al) atoms and are of catalytic importance [36].

The specific peak area is proportional to the number of acid sites in the sample and can be determined by integration by convolution of the area under the curve of the spectra. The amounts of strong and weak acid sites are listed in Table 4. The acid site density increased in the order MCM-68 <TNU-9 < MCM-22.

3.7 Solid State NMR Spectroscopy (^{27}Al and ^{29}Si MAS NMR)

Figure 8a shows the ^{27}Al MAS NMR spectra of M22-30A, M22-30A 0.01 Zn-G, and ZnM22-30A. Figure shows two peaks at 54 ppm and 0 ppm, corresponding to tetrahedral Al (Al_F) entering the zeolite framework and extra-framework

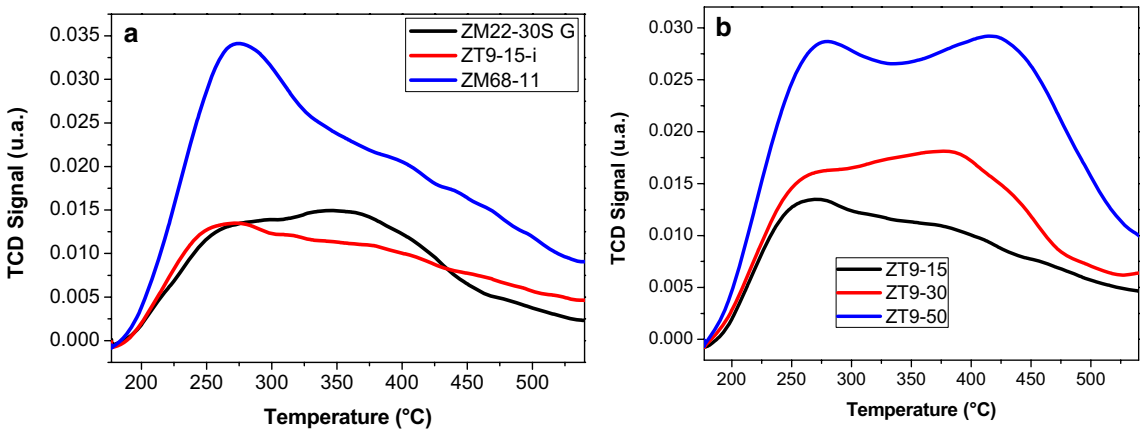

Fig. 7 NH_3-TPD profiles of **a** three structure zeolitic and **b** TNU-9 modified-Zn zeolites with different Si/Al ration

Table 4 Acidity properties of materials

Catalyst	Acidity (μmol NH_3/g)		
	Weak acid (LT)	Strong acid (HT)	Total
M22-30A	5134	–	5134
M22-30S	4918	–	4918
ZM22-30AG	6834	–	6834
M22-50A	5692	–	5692
M22-50S	6975		6975
ZM68-11	14,549	–	14,549
T9-15	7929	–	7929
ZT9-15	9978	–	9978
T9 0.5 Zn	9531	–	9531
T9 0.2 Zn	13,388	–	13,388
T9-30	8983	–	8983
ZT9-30	1729	4595	6324
T9-50	8162	–	8162
ZT9-50	3235	6184	9419

octahedral Al atoms (Al_{EF}), respectively. The small shoulder around 56 ppm is attributed to the Al species located at crystallographically different T sites [37]. However, the peaks intensity of Al_{EF} y Al_F decreased slightly due incorporation of Zn. That result demonstrate that the Zn cations could cover Al sites in octahedral and tetrahedral positions.

Figure 8b shows the ^{27}Al MAS NMR spectra of the acid form of TNU-9 (Si/Al 15) and modified with Zn. The both spectra feature a strong chemical shift at 54 ppm and a weak chemical shift at 0 ppm, corresponding to tetrahedrally coordinated aluminum in the framework and octahedrally coordinated aluminum extra-framework, respectively [38]. The signal at 0 ppm are ascribed to extra-framework aluminum from either cationic aluminum hydroxide species/hydroxylated alumina-like clusters inside the channel structure or as framework defects, where hydroxyl groups and water are partly bonded [39, 40]. It is observed that after the exchange with Zn the peak corresponding to the Al_{EF} decreases, which indicates that the Zn could occupy sites in octahedral positions of the Al. This indicates AL_{EF} sites are incorporated into the framework structure and that defect sites are annealed by the ion exchange treatment, since the amounts of octahedral Al is reduced [39].

The ^{29}Si MAS-NMR spectra of MCM-22 structure and modified samples are presented in Fig. 9a. According to the literature, in the MCM-22 framework there are 8 crystallographically non-equivalent T-atoms [33] giving equal number of ^{29}Si MAS-NMR resonances. The Q4 environments [that is, $T(TO)_4$ groups] resonant at ca. – 105, – 110, – 111, – 112, – 114, – 115 and – 119.5 ppm, while the Q3 sites (that is, $T(TO)_3(OH)$ groups) give peaks at – 104 and – 100 ppm [24, 40–42].

All the MCM-22 spectra show five signals in the Q4 region (– 120.0, – 114.7, – 112.6, – 106.6) and an additional one inside the Q3 region in – 100 ppm, the latter being due to silanol groups.

^{29}Si MAS NMR spectrum of the T9-15 and ZT9-15 samples indicates the presence of only $Si(OSi)_4$ sites with a relative intensity in – 105.1 to – 111.1 ppm [16] (Fig. 9b). This may largely be attributed to the ZnO clusters, which cover partial $(OH)Si(OSi)_3$ species on the framework of zeolite [37].

Figure S3a (Supplementary Material S3) shows the ^{27}Al MAS NMR spectra of all the TNU-9 modified-Zn samples with different ration Si/Al. Both tetrahedral (Al^{IV}, signals around 56 ppm) and octahedral (Al^{VI}, signal at 0 ppm) Al species are present in all samples and the amount of extra-framework Al species increased with the Al content in the

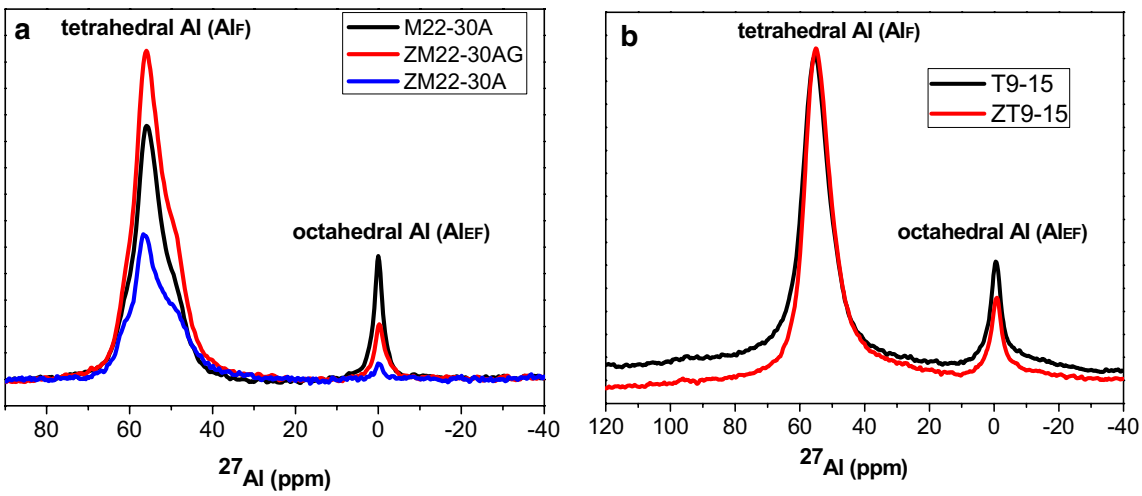

Fig. 8 ^{27}Al MAS NMR spectra of **a** MCM-22 modified (Si/Al 30) materials and **b** acid and Zn-modified TNU-9 zeolite (Si/Al 15)

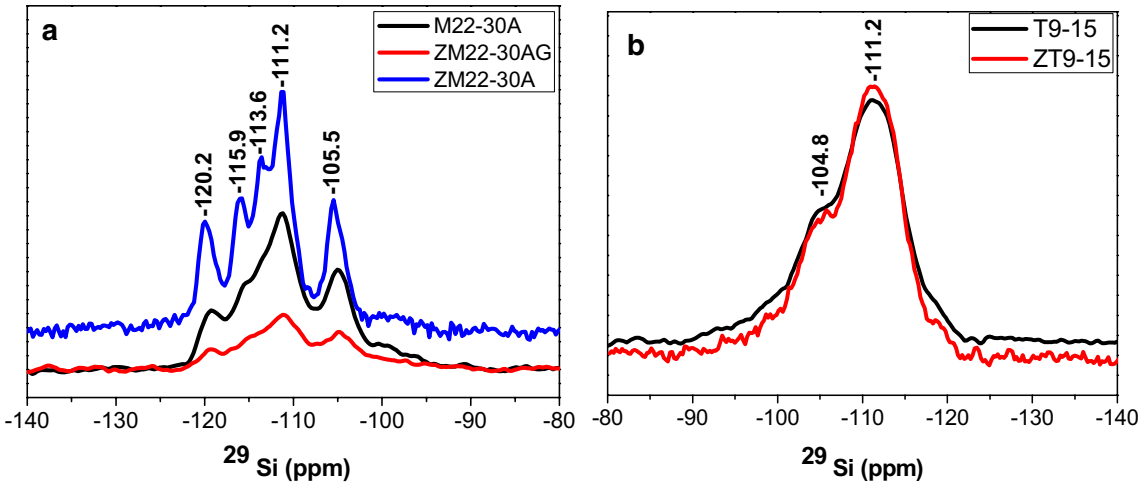

Fig. 9 ^{29}Si MAS NMR spectra of **a** MCM-22 materials (Si/Al 30) and **b** acid and modified TNU-9 zeolite (Si/Al 15)

sample [42, 43]. On the other hand, Figure S3b shows the ^{29}Si MAS NMR spectra of all the ZT9 samples modified with Zn. It is observed that by increasing the Si/Al ration the intensity of the signal at − 111.1 increases considerably. The peak at 105.1 ppm disappears in the samples ZT9-30 and ZT9-50, however, a peak appears around 109 ppm in both cases.

3.8 Catalytic Evaluation

From literature it is known that catalyst stability in the MTA reaction is also influenced by acid site density, crystal size and acid site strength [44]. The catalytic activity and selectivity of T9-15 and ZT9-15 samples are shown in Fig. 10a and b, with conditions of 400 °C, WHSV 4.24 h^{-1} and 0.5 g of catalysts. The introduction of zinc species as well as the synthesis method exhibits a significant influence on the catalyst lifetime, methanol conversion, and product distribution. Both catalysts showed high conversion initial at 400 °C (Fig. 10a), full conversion of oxygenates (both methanol and intermediate dimethylether, DME) was obtained, however, the clear distinction into both of stabilities, with ZT9-15 deactivating rapidly after 5 h of reaction and T9-15 deactivating slowly, only correlates with the presence of Zn and the formation new acid sites produced by divalent metal. The 3D channel system with cavity structure allows TNU-9 to better generate, accommodate and diffuse of aromatics in the reaction. The presence of cavities in TNU-9 can accommodate more Zn species in the channels associated to Brønsted acid sites [45, 46]. Selectivity to short chain olefins (C2 to C4) reached a nearly constant level close to 40% after until 5 h on stream (Fig. 10b). The selectivity to total aromatics

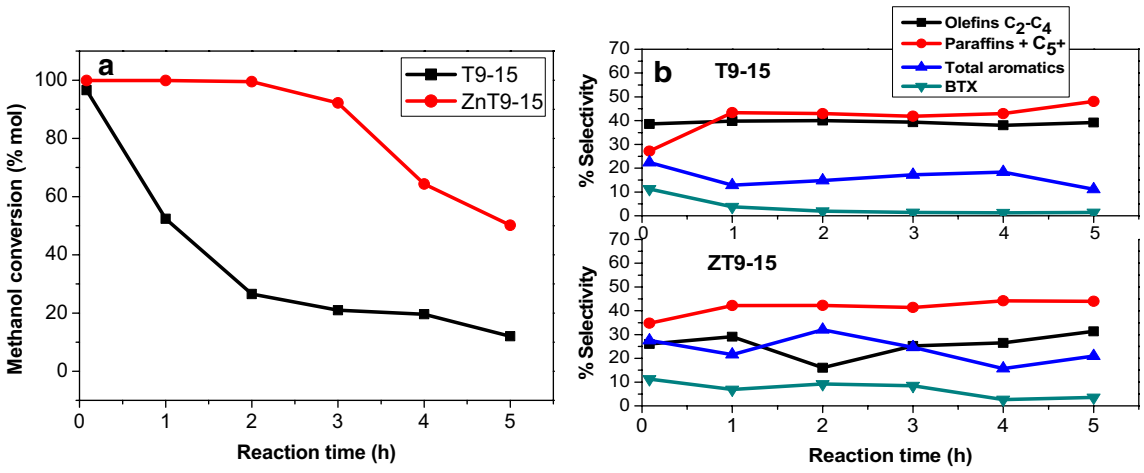

Fig. 10 **a** Methanol conversion and **b** selectivity to compounds vs. reaction time obtained with T9-15 and ZT9-15 catalysts. Test conditions: T = 400 °C, WHSV = 4.24 h^{-1}, 0.5 g of catalyst

improved significantly with the incorporation of Zn into the ZT9-15 zeolite during the 5 h reaction.

3.8.1 Effect of Structure on the MTH Reaction

The compared three 3D 10-ring topologies, two with 10-rings extended channel (MWW and TNU-9) and one combined channels of 10 and 12 rings (MSE) were listed in Table 5 in TOS 1 h and WHSV of 4.24 h^{-1} and 400 °C. The introduction of zinc species exhibits a significant influence on the catalyst lifetime, methanol conversion, and product distribution. The topology of each of the catalysts had a significant influence on the catalytic activity, all catalysts gave initially full methanol conversion at 1 h of reaction, however, the zeolite TNU-9 in ration Si/Al 15 showed a greater selectivity to the BTX fraction (6.87%) compared to the other two structures due the TNU-9 zeolite possesses the largest cavity and provides the Brønsted sites of the highest strength [47]. The main reason is the size of cavities formed by channel intersections. Larger cavities in TUN-9 zeolite lead to aromatics formation compared to MCM-22 zeolite [48]. Furthermore, MCM-68 zeolite contained mainly heavy aromatics, due to its high acidity and the space of its supercages of up to 18 members. Large empty space gives rise to the formation of larger molecules, mainly C9–C12 (aromatics with carbon number nine and higher). Heavy aromatics act as coke precursors, thus, their formation should be limited. The MCM-22 zeolite has a 10-ring system, so that the reaction proceeds higher olefins and paraffins selectivity and lower aromatics selectivity (20.05%), this due to the peculiar pore structure of MCM-22 zeolite (10 and 12 MR channels). This result indicates that the cavity size of 3D 10-ring zeolites is of primary importance for their stability as MTH catalysts. It should be noted that, when considering the pore size of TNU-9 have clearly larger channels than the other topologies. The 3D channel system with cavity structure allows TNU-9 to better generate, accommodate and diffuse of aromatics in the reaction. In addition, we have also found that the presence of supercage favors the diffusion and migration of Zn species into the channels associated to Brønsted acid sites and improves activity and stability in MTH process. The selectivity total aromatics over several catalysts under this study, followed the order: ZM68-11 > ZT9-15 > ZM22-30A.

Table 5 Distribution of reaction products of different structures in the conversion of methanol

Catalyst	ZT9-15	ZM68-11	ZM22-30A
Methanol conversion (mol %)	99.70	90.36	99.27
Selectivity to products (% mol)			
Olefins C_2–C_4	29.09	25.76	26.64
Paraffins + olefins C_5^+	42.19	41.87	53.31
Bencene	0.18	0.07	0.03
Toluene	1.46	0.06	0.57
Xilenes	5.23	0.24	2.28
Total aromatics	28.72	32.36	20.05
BTX total	6.87	0.37	2.88

Conditions: TOS 1 h, WHSV 4.24 h^{-1}, 400 °C

3.8.2 Effects of Temperature on the Catalytic Performance of Zn/TNU-9 Catalysts

The effect of temperature reaction on the catalytic performance of T9-15 0.5 Zn modified-Zn catalysts is shown in Fig. 11a and b. It is observed that the temperature affects the useful life of the catalyst, as the reaction temperature increases the catalyst tends to deactivate. When increasing the temperature reaction, the conversion of methanol decreased after 5 h at 425 and 450 °C. At 400 °C, the conversion is constant during 9 h of reaction, in the opposite case at 450 °C, where the conversion decreased to 20% after 8 h of reaction, indicating catalyst deactivation. These results suggest that the catalyst did not display perfect catalytic stability in methanol reaction to 450 °C. A high temperature more carbonaceous deposits were formed, and the coke can cover the active sites, which may induce a short lifetime of the catalyst. However, with an increase of the reaction temperature, the selectivity to BTX increased at initial time (Fig. 11b). These results suggest that an increase in the reaction temperature, specifically at 450 °C, favored the aromatization of methanol, however, to higher reaction temperature suppressed dehydrocyclization and promoted the formation of coke from a secondary reaction [49], indicating that the cokes on the T9-15 0.5 Zn probably do not cover the active sites and the channels for the reactants and BTX products are not blocked to a low temperature. In addition to temperature, particle size and particle density and kind of active sites on the crystallite surface will be of influence on catalyst lifetime [49, 50].

On other hand, comparison of the T9-15 catalysts with the ration $ZnO/ZnO + Al_2O_3$ equal to 0.34 and 0.16 were made at 400 °C and WHSV of 4.24 h^{-1} were realized. The first one (T9-15 0.5 Zn) showed better stability with conversion of methanol completes during 9 h of reaction. T9-15 0.2 Zn catalyst presented lower conversion of methanol after 9 h, around 80% mol. Also, this last catalyst showed better BTX selectivity (17%) at short reaction times (black line), T9-15 0.2 Zn (red line) presented a lower BTX selectivity (around 5% during all the reaction). It the higher BTX selectivity over the T9-15 0.5 Zn catalyst is perhaps related to its distinctive channel systems, which can accommodate more Zn species in the zeolite channels associated to Brønsted acid sites. This suggests the highly dispersed nature of its zinc particles.

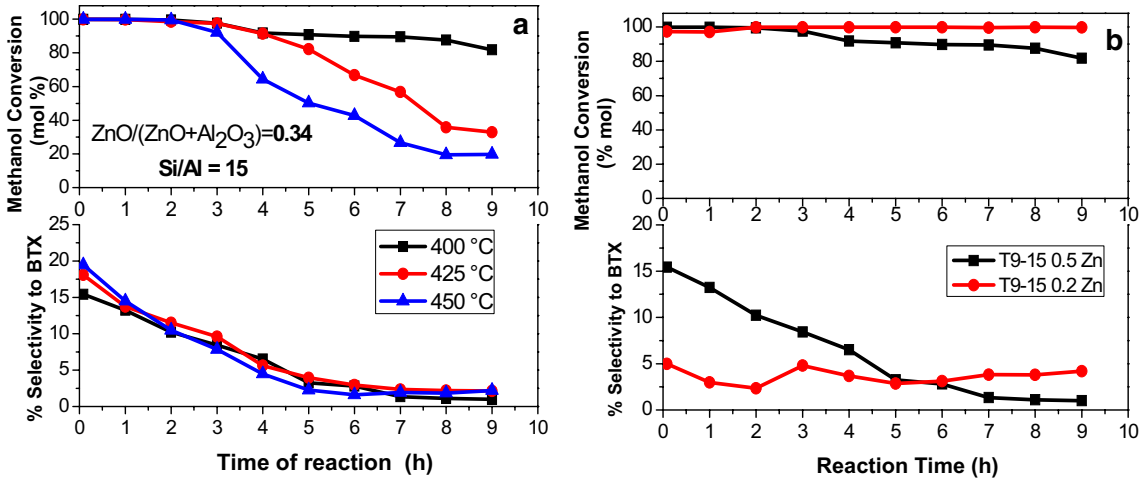

Fig. 11 **a** Methanol conversion and Selectivity to BTX with T9-15 0.5 Zn to 400, 425 and 450 °C. **b** Comparation selectivity to compounds vs. reaction time obtained with T9-15 and ZT9-15 catalysts. Test conditions: T = 400 °C, WHSV = 4.24 h^{-1}, 0.5 g of catalyst

The BTX formation over H-TNU-9 would occur mainly inside the two types of 10-ring channels along [010] rather than inside its large 12-ring cavities [17, 48].

Figure 12a and b show the effects of the reaction temperature of T9-30 and ZT9-30 with a WHSV 4.24 h^{-1}, respectively. Figure 12a shows that the methanol was nearly completely converted to 400 and 425 °C until 5 h of reaction, decreasing to 85% in both cases. The conversion of methanol decreased to 80% after 5 h of reaction to 450 °C, however, total aromatics selectivity increased to short reaction time (80%) and subsequently decreased after 5 h to reaction. So, at 450 °C the acid sites are activated in the MTA reaction. In contrast, the acid zeolite had a low selectivity to total aromatics to short time at three temperatures compared to the zeolite exchanged with Zn.

3.8.3 Effect of Zn Incorporation Method on TNU-9 Catalysts

In this work the Zn has been incorporated to the zeolite by synthesis or by ion-exchange, as detailed in the experimental part. In a previous study, we have demonstrated that the impregnation method, commonly used to incorporate different cations or metals to catalysts, was not effective to improve the stability of Zn-modified catalysts for MTH [10]. These catalysts suffer a rapid deactivation probably because during the impregnation process an accumulation of a small amount of nanometric ZnO clusters occurs in the channels of zeolite, avoiding the aromatics diffusion and accelerating the catalyst deactivation due to coke deposition. In addition, the selectivity to aromatic compounds was considerably lower.

The results of the conversion of methanol with different TNU-9 catalysts modified-Zn to 400 °C are presented in

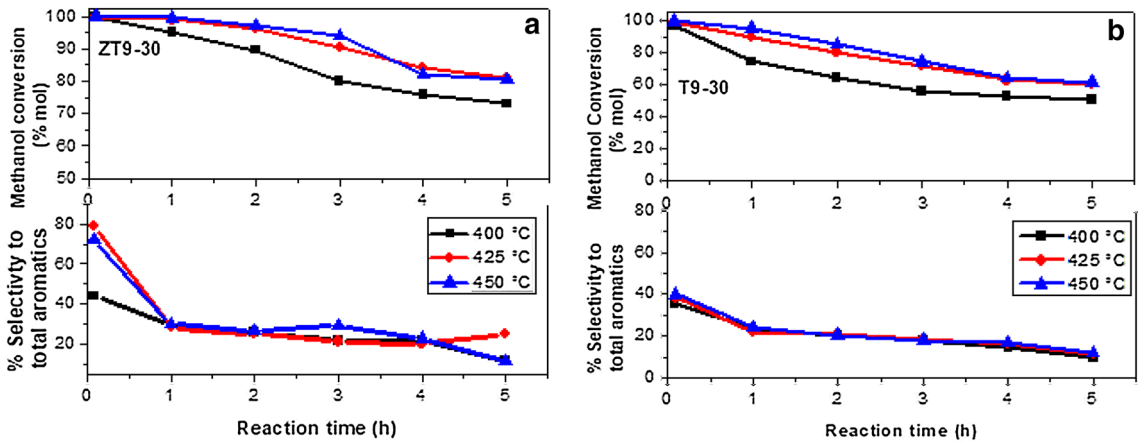

Fig. 12 Methanol conversion and selectivity to total aromatics vs time of **a** ZT9-30 and **b** ZT9-30 (acid zeolite) to different temperature 400, 425 and 450 °C Test conditions: WHSV = 4.24 h^{-1}, 0.5 g of catalyst

Table 6. In this study, the BTX selectivity at 1 h of reaction increased in the order T9-15 0.5 Zn > ZT9-15 T9-15 > T9-15 0.2 Zn, which is also in agreement with the observed relative stability. The least active and selective was TNU-9 acid zeolite providing the Si(OH)Al groups of the highest strength but accommodating the largest cavities on the intersection of 10-ring channels with lower selectivity BTX and total aromatics, 3.77 and 16.82%, respectively [47]. HT9 0.5 Zn zeolite was the better catalyst for total aromatics and BTX selectivity (12.58%) due high acid density and high account of Zn, which is an aromatizing agent. This suggests that most of the acid sites in the proton form originates from the presence of both Al and Zn in framework positions using ration $ZnO/ZnO + Al_2O_3$ equal to 0.34. In our work demonstrated that activity of Zn-modified TNU-9 zeolites in the MTA reaction improves by prepared using ration $ZnO/ZnO + Al_2O_3$ of 0.34 (T9-15 0.5 Zn) and demonstrated significantly higher selectivity for aromatics compared with acid zeolite.

On the other hand, the incorporation of zinc species by ion exchanging (ZM22-30S-G) and synthesis gel (ZM22-30S) in MCM-22 zeolite has high influence on the catalytic stability methanol conversion, and products distribution to 400 °C (Figure S4a and b). The first one showed lower methanol conversion after 5 h of reaction (20%), the exchanged zeolite presented better conversion of methanol values, 80% mol during of 5 h of reaction. Which is usually associated with diffusion limitations of heavy products by the formation of large Zn species formed in the micropores [51].

However, the incorporation of zinc by ion exchange increases the formation of aromatic compounds (blue line) obtaining selectivity around 20 and 30% during the reaction (Figure S5a), contrary case ZM22-30S-G, which presented selectivity less than 20%. In addition, the selectivity of light olefins and paraffins were showed, which were not modified with the incorporation of Zn in the zeolites.

Table 6 Distribution of reaction products of HTNU-9 materials modified-Zn (Si/Al 15) in the conversion of methanol

Catalyst	T9-15	ZT9-15	T9 0.5 Zn	T9 0.2 Zn
Methanol conversion (mol %)	99.70	89.37	99.85	81.09
Selectivity to products (% mol)				
Olefins C_2–C_4	39.83	29.09	28.30	18.95
Paraffins + olefins C_5^+	43.36	42.19	36.82	50.59
Bencene	0.06	0.18	0.73	0.10
Toluene	0.47	1.46	4.13	0.64
Xilenes	3.24	5.23	7.72	2.24
Total aromatics	16.82	28.72	34.88	30.56
BTX fraction	3.77	6.87	12.58	2.98

Conditions: TOS 1 h, WHSV 4.24 h^{-1}, 400 °C

3.8.4 Effects of the Morphology on the MCM-22 Catalysts

From literature it is known that catalyst stability in the MTH reaction is also influenced by acid site density and this case the crystal size. The conversion of methanol and the distribution of reaction products of the MCM-22 zeolite with different synthesis conditions (agitation and static) and therefore with different morphology are shown in Fig. 13a and b, respectively. The M22-30S zeolite showed higher conversion levels compared to the M22-30A zeolite due under static conditions (M22-30S) smaller particles (1.5 µm) are obtained, in contrast to static conditions when obtaining larger particles (about 7 µm) as observed by SEM. The generation of smaller crystals influences the optimization of

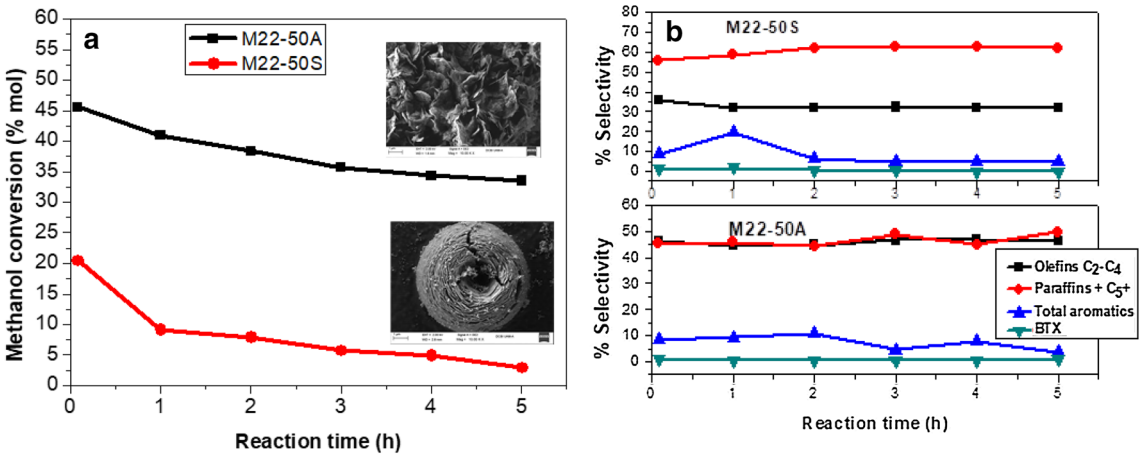

Fig. 13 Morphology effect in catalytic activity **a** Methanol conversion (% mol) M22-50A (agitation condition) and M22-50S (static condition). **B** Selectivity to total compounds vs time. Test conditions: T = 400 °C, WHSV = 4.24 h^{-1}, 0.5 g of catalyst

the acid properties of zeolite to enhance the catalytic activity making shortens the length of diffusion of molecules [28, 52]. In terms of selectivity, the zeolites were selective for obtaining light olefins and paraffins, this corresponds to what was reported by several researchers and low acidity measured by TPD-NH_3. Min et al. [53] found that contribution of supercages and their sinusoidal 10-ring channels are responsible for the high activity in the MTO reaction. Zhang et al. [18] also mention the light olefins selectivity seems to be related to the amounts of Brønsted acid sites present in the MCM-22 zeolite. Similarly, the selectivity to olefins and paraffins benefits from the presence of smaller size such as zeolite M22-30A. In our work, improved aromatization of methanol results was observed when converting methanol using three zeolites Zn-modified compared to other works previously studied by other authors [44, 18, 54] and all gave good MTA ability but the BTX selectivity less than those obtained by us. Additionally, zeolite TNU-9 has been poorly studied in this reaction.

4 Conclusions

TNU-9, MCM-22 and MCM-68 are all active for the conversion of methanol at different temperatures, however, the distribution of reaction products was different for each zeolite. MTH reaction is also influenced by acid site density, crystal size and acid site strength. TNU-9 zeolite is an active catalyst for the studied reactions related to BTX aromatics, comparable to other zeolites studied in this work, mainly due to its acidic and topological characteristics. The Zn incorporation had influences on the textural properties, morphology, acidic properties and catalytic performances for all zeolites. T9-15 0.5 Zn zeolite showed a high content of total aromatics and therefore high selectivity to the BTX fraction. The BTX selectivity was effectively improved by introduction of Zn species by ion exchange in the case of ZT9-30 zeolite, due to a greater distribution of strong acid sites, the generation of strong acid sites were the active sites for the conversion of MTA. The reaction temperature has great influence on the catalytic activity in ZT9-30 zeolite, at 450 °C the best BTX selectivity is obtained, however, the catalyst is deactivated after 9 h of reaction. The crystal size parameter to affect the catalyst lifetime of the three topologies studied. In methanol conversion, the selectivity to aromatics over the T9-15 (Si/Al 15) zeolite catalysts under study, follow the order: T9-15 0.5 Zn > ZT9-15 T9-15 > T9-15 0.2 Zn. T9-15 catalysts with the ration $ZnO/ZnO + Al_2O_3$ equal to 0.34 (T9-15 0.5 Zn) at 400 °C and WHSV of 4.24 h^{-1} presented the best total aromatic selectivity (32%) at 1 h of reaction. In terms of zeolite topology, aromatic selectivity increased in the following order. ZM68-11 > ZT9-15 > ZM22-30, however, MCM-68 zeolite modified-Zn produced mainly heavy aromatics, due to its high acidity and the space of its super-cages of up to 18 members. Finally, MCM-22 zeolites, regardless of morphology, were selective for obtaining light olefins and paraffins, due to its structure formed by supercages and their sinusoidal 10-ring channels, as well as its low acidity.

The different between the three tested topologies with respect to products selectivities and methanol conversion is a clear evidence of the importance of the channel dimensions in the MTH reaction. The zeolite MCM-68 presented a generation of heavy hydrocarbons (C9–C12) which were responsible for the generation of coke causing the rapid deactivation of the catalyst due to 12-member and clearly channels larger channels than the other topologies. The unique pore architecture and strong acid of zeolite TNU-9, with 10-ring channel systems, being slightly larger zeolite compared with MCM-22, can offer new opportunities for methanol conversion.

Acknowledgements The authors thank the Spanish Research Agency -AEI- and the European Regional Development Fund -FEDER- for the financing of this work, through the Project MAT2016-77496-R (AEI/FEDER, EU). MGR thanks the Molecular Sieve Group of the Institute of Catalysis and Petrochemistry (CSIC) in Madrid and CONACyT for the support granted for the research stay in Spain.

Author Contributions All authors contributed to the study conception and design. Material preparation, data collection and analysis were performed by Dora A. Solís Casados, Julia Aguilar Pliego, Carlos Márquez Álvarez, Enrique Sastre de Andrés, Diana Sanjurjo Tartalo, Raquel Sáinz Vaque and Marisol Grande Casas. The first draft of the manuscript was written by PhD student, Misael Garcia Ruiz and all authors commented on previous versions of the manuscript. All authors read and approved the final manuscript.

Compliance with Ethical Standards

Conflict of interest The authors declare that they have no conflict of interest.

Research Involving Human Participants and/or Animals This work does not contain any studies with human participants or animals performed by any of the authors.

Informed Consent Finally, additional informed consent was obtained from all individual participants for whom identifying information is included in this chapter.

References

1. Zhu X (2015) Hierarchical zeolites as catalysts for methanol conversion reactions. Technische Universiteit Eindhoven, Eindhoven
2. Blomsma E, Martens JA, Jacobs PA (1997) Isomerization and hydrocracking of heptane over bimetallic bifunctional PtPd/H-beta and PtPd/USY zeolite catalysts. J Catal 165(2):241–248
3. Fraenkel D, Cherniavsky M, Ittah B, Levy M (1986) Shape-selective alkylation of naphthalene and methylnaphthalene with methanol over H-ZSM-5 zeolite catalysts. J Catal 101(2):273–283

4. Zhang GQ, Bai T, Chen TF, Fan WT, Zhang X (2014) Conversion of methanol to light aromatics on Zn-modified nano-HZSM-5 zeolite catalysts. Ind Eng Chem Res 53:14932–14940
5. Zhang J, Qian W, Kong C, Wei F (2015) Increasing para-Xylene Selectivity in Making Aromatics from Methanol with a surface-modified Zn/P/ZSM-5 catalyst. ACS Catal 5(5):2982–2988
6. Wang T, Tang X, Huang X, Qian W, Cui Y, Hui X, Yang W, Wei F (2014) Conversion of methanol to aromatics in fluidized bed reactor. Catal Today 233:8–13
7. Baliban RC, Elia JA, Floudas CA (2013) Biomass to liquid transportation fuels (BTL) systems: process synthesis and global optimization framework. Energy Environ Sci 6:267–287
8. Appelt J, Heschel W, Meyer B (2016) Catalytic pyrolysis of central German lignite in a semi-continuous rotary kiln—performance of pulverized one-way ZSM-5 catalyst and ZSM-5-coated beads. Fuel Process Technol 144:56–63
9. Bjørgen M, Joensen F, Holm MS, Olsbye U, Lillerud KP, Svelle S (2008) Methanol to gasoline over zeolite H-ZSM-5: improved catalyst performance by treatment with NaOH. Appl Catal A 345:43–50
10. Garcia-Ruiz M, Solis-Casados DA, Aguilar-Pliego J, Márquez-Álvarez C, Sastre de Andrés E, Sanjurjo-Tartalo D, Sainz-Vaque R, Grande-Casas M (2020) ZSM-5 zeolites modified with Zn and their effect on the crystal size in the conversion of methanol to light aromatics (MTA). React Kinet Mech Catal. https://doi.org/10.1007/s11144-019-01716-4
11. Yubing X, Puyu Q, Xinping D, Haiqiang L, Youzhu Y (2013) Enhanced performance of Zn–Sn/HZSM-5 catalyst for the conversion of methanol to aromatics. Catal Lett 143:798–806
12. Gabrienko AA, Arzumanov SS, Toktarev AV, Danilova IG, Prosvirin IP, Kriventsov VV, Zaikovskii VI, Freude D, Stepanov AG (2017) Different efficiency of Zn^{2+} and ZnO species for methane activation on Zn-modified zeolite. ACS Catal 7(3):1–45
13. Ma D, Shu Y, Han X, Liu X, Xu Y, Bao X (2001) Mo/HMCM-22 catalysts for methane dehydroaromatization: a multinuclear MAS NMR Study. J Phys Chem B 105:1786–1793
14. Dorset DL, Weston SC, Dhingra SS (2006) Crystal structure of ZEOLITE MCM-68: a new three-dimensional framework with large pores. J Phys Chem B 110:2045–2050
15. Ni Y, Sun A, Wu X, Hai G, Hu J, Li T, Li G (2011) The preparation of nano-sized H[Zn, Al]ZSM-5 zeolite and its application in the aromatization of methanol. Micropor Mesopor Mater 143:435–442
16. Hong SB, Lear EG, Wright PA, Zhou W, Cox PA, Shin CH, Park JH, Nam IS (2004) Synthesis, structure solution, characterization, and catalytic properties of TNU-10: a high-silica zeolite with the STI topology. J Am Chem Soc 126:5817–5826
17. Hong SB, Nam IS, Min HK, Shin CH, Warrender SJ, Wright PA, Cox PA, Gramm F, Baerlocher Ch, McCusker LB, Liu Z, Ohsuna T, Terasaki O (2007) TNU-9: a novel medium-pore zeolite with 24 topologically distinct tetrahedral sites. Zeolites to Porous MOF Materials—the 40th Anniversary of International Zeolite Conference
18. Zhang L, Wang H, Liu G, Gao K, Wu J (2016) Methanol-to-olefin conversion over H-MCM-22 catalyst. J Mol Catal A 411:311–316
19. Wu Y, Ren X, Lu Y, Wang J (2008) Crystallization and morphology of zeolite MCM-22 influenced by various conditions in the static hydrothermal synthesis. Micropor Mesopor Mater 112:138–146
20. Hao H, Chang Y, Yu W, Lou LL, Liu S (2018) Hierarchical porous MCM-68 zeolites: synthesis, characterization and catalytic performance in m-xylene isomerization. Micropor Mesopor Mater 263:135–141
21. Calabro JC, Cheng RA, Crane Jr, Kresge CT, Dhingra SS, Steckel MA, Stern DL. Weston SC (2000) U. S. Patent. 6049018
22. Kubu M, Zones SI, Cejka J (2010) TUN, IMF and -SVR zeolites; synthesis. Prop Acid Top Catal 53:1330–1339
23. Corma A, Corell C, Pérez-Pariente J (1995) Synthesis and characterization of the MCM-22 zeolite. Zeolites 15(1):2–8
24. Delitala C, Alba MD, Becerro AI, Delpiano D, Meloni D, Musu E, Ferino I (2009) Synthesis of MCM-22 zeolites of different Si/Al ratio and their structural, morphological and textural characterization. Micropor Mesopor Mater 118:1–10
25. Tian ZR, Voigt JA, Liu J, Mckenzie B, Mcdermott MJ, Rodriguez MA, Konishi H, Xu H (2003) Complex and oriented ZnO nanostructures. Nat Mater 2:821–826
26. Li J, Lou LL, Yang Y, Hao H, Liu S (2015) Alkylation of phenol with tert-butyl alcohol over dealuminated HMCM-68 zeolites. Micropor Mesopor Mater 207:27–32
27. Hu J, Wu S, Liu H, Ding H, Li Z, Guan J, Kan Q (2014) Effect of mesopore structure of TNU-9 on methane dehydroaromatization. RSC Adv 4:26577–26584
28. Ji Y, Yang H, Yan W (2017) Strategies to enhance the catalytic performance of ZSM-5 zeolite in hydrocarbon cracking: a review. Catalysts 7(367):1–31
29. Ernst S, Elangovan SP, Gerstner M, Hartmann M, Hecht T, Sauerbeck S (2004) Characterization and catalytic evaluation of zeolite MCM-68. Stud Surf Sci Catal 154:2861–2868
30. Su X, Wang G, Bai X, Wu W, Xiao L, Fang Y, Zhang J (2016) Synthesis of nanosized HZSM-5 zeolites isomorphously substituted by gallium and their catalytic performance in the aromatization. Chem Eng 293:365–375
31. Jung HJ, Park SS, Shin CH, Park YK, Hong SB (2007) Comparative catalytic studies on the conversion of 1-butene and n-butane to isobutene over MCM-22 and ITQ-2 zeolites. J Catal 245:65–74
32. Topsøe N, Pedersen K, Derouane E (1981) Infrared and temperature-programmed desorption study of the acidic properties of ZSM-5-type zeolites. J Catal 70:41–52
33. Wu P, Kan Q, Wang X, Wang D, Xing H, Yang P, Wu T (2005) Acidity and catalytic properties for methane conversion of Mo/HZSM-5 catalyst modified by reacting with organometallic complex. Appl Catal A 282:39–44
34. Joly JF, Ajot H, Merlen E, Raatz F, Alario F (1991) Parameters affecting the dispersion of the gallium phase of gallium H-MFI aromatization catalysts. Appl Catal A 79:249–263
35. Xiaoning W, Zhen Z, Chunming X, Aijun D, Li Z, Guiyuan J (2007) Effects of fight rare earth on acidity and catalytic performance of HZSM-5 zeolite for catalytic clacking of butane to light olefins. J Rare Earths 25:321–328
36. Reddy JK, Motokura K, Koyama T, Miyaji A, Baba T (2012) Effect of morphology and particle size of ZSM-5 on catalytic performance for ethylene conversion and heptane cracking. J Catal 289:53–61
37. Kolodziejski W, Zicovich-Wilson C, Corell C, Perez-Pariente J, Corma A (1995) ^{27}Al and ^{29}Si MAS NMR Study of Zeolite MCM-22. J Phys Chem 99(18):7002–7008
38. Song YQ, Feng YL, Liu F, Kang CL, Zhou XL, Xu LY, Yu GX (2009) Effect of variations in pore structure and acidity of alkali treated ZSM-5 on the isomerization performance. J Mol Catal A 310:130–137
39. Pinilla-Herrero I, Borfecchia E, Holzinger J, Mentz UV, Finn J, Lomachenko KA, Bordiga S, Lamberti C, Berlier G, Olsbye U, Svelle S, Skibsted J, Beato P (2018) High Zn/Al ratios enhance dehydrogenation vs hydrogen transfer reactions of Zn-ZSM-5 catalytic systems in methanol conversion to aromatics. J Catal 362:146–163
40. Saito H, Inagaki S, Kojima K, Han Q, Yabe T, Ogo S, Kubota Y, Sekine Y (2018) Preferential dealumination of Zn/H-ZSM-5 and its high and stable activity for ethane dehydroaromatization. Appl Catal A 549:76–81

41. Machado V, Rocha J, Carvalho AP, Martins A (2012) Modification of MCM-22 zeolite through sequential post-synthesis treatments. Implications on the acidic and catalytic behavior. Appl Catal A 445:329–338
42. Elyassi B, Zhang X, Tsapatsis M (2014) Long-term steam stability of MWW structure zeolites (MCM-22 and ITQ-1). Micropor Mesopor Mater 193:134–144
43. Wang P, Huang L, Li J, Dong M, Wang J, Tatsumi T, Fan W (2015) Catalytic properties and deactivation behavior of H-MCM-22 in the conversion of methanol to hydrocarbons. RSC Adv 5:1–28
44. Bleken F, Skistad W, Barbera K, Kustova M, Bordiga S, Beato P, Lillerud KP, Svellea S, Olsbye U (2011) Conversion of methanol over 10-ring zeolites with differing volumes at channel intersections: comparison of TNU-9, IM-5, ZSM-11 and ZSM-5. Phys Chem Chem Phys 13:2539–2549
45. Franch-Martí C, Alonso-Escobar C, Jorda JL, Peral I, Hernández-Fenollosa J, Corma A, Palomares AE, Rey F, Guilera G (2012) TNU-9, a new zeolite for the selective catalytic reduction of NO: an in situ X-ray absorption spectroscopy study. J Catal 295:22–30
46. Al-Khattaf S, Ali SA, Aitani MA, Žilková N, Kubicka D, Cejka J (2014) Recent advances in reactions of alkylbenzenes over novel zeolites: the effects of zeolite structure and morphology. Catal Rev 56:333–402
47. Gołąbek K, Tarach KA, Filek U, Góra-Marek K (2018) Ethylene formation by dehydration of ethanol over medium pore zeolites. Spectrochim Acta A 192:464–472
48. Liu H, Yang S, Wu S, Shang F, Yu X, Xu C, Guan J, Kan Q (2011) Synthesis of Mo/TNU-9 (TNU-9 Taejon National University No. 9) catalyst and its catalytic performance in methane non-oxidative aromatization. Energy 36:1582–1589
49. Zhao YH, Gao TY, Wang YJ, Zhou YJ, Huang GQ (2018) Zinc supported on alkaline activated HZSM-5 for aromatization reaction. React Kinet Mech Cat 125(2):1085–1098
50. Schulz H (2010) "Coking" of zeolites during methanol conversion: Basic reactions of the MTO- MTP- and MTG processes. Catal Today 154:183–194
51. Olsbye U, Svelle S, Bjørgen M, Beato P, Janssens T, Bordiga S, Lillerud K (2012) Conversion of methanol to hydrocarbons: how zeolite cavity and pore size controls product selectivity. Angew Chem Int Ed 51:2–24
52. Petushkov A, Yoon S, Larsen SC (2011) Synthesis of hierarchical nanocrystalline ZSM-5 with controlled particle size and mesoporosity. Micropor Mesopor Mat 137:92–100
53. Min KH, Park MB, Hong SB (2010) Methanol-to-olefin conversion over H-MCM-22 and H-ITQ-2 zeolites. J, Catal 271:186–194
54. Lacarriere A, Luck F, Swierczynski D, Fajula F, Hulea V (2011) Methanol to hydrocarbons over zeolites with MWW topology: Effect of zeolite texture and acidity. Appl. Catal. A-Gen. 402:208–217